A micromechanics-based mesomodel for unidirectional laminates in compression

Nicolas Feld, Olivier Allix, Emmanuel Baranger, Jean-Mathieu Guimard

▶ **To cite this version:**

Nicolas Feld, Olivier Allix, Emmanuel Baranger, Jean-Mathieu Guimard. A micromechanics-based mesomodel for unidirectional laminates in compression. 3rd ECCOMAS Thematic Conference on the Mechanical Response of Composites, Sep 2011, Hannover, Germany. pp.61-68. hal-00667171

HAL Id: hal-00667171
https://hal.science/hal-00667171

Submitted on 7 Feb 2012

HAL is a multi-disciplinary open access archive for the deposit and dissemination of scientific research documents, whether they are published or not. The documents may come from teaching and research institutions in France or abroad, or from public or private research centers.

L'archive ouverte pluridisciplinaire **HAL**, est destinée au dépôt et à la diffusion de documents scientifiques de niveau recherche, publiés ou non, émanant des établissements d'enseignement et de recherche français ou étrangers, des laboratoires publics ou privés.

A micromechanics-based mesomodel for unidirectional laminates in compression

N. Feld[1], O. Allix[1], E. Baranger[1], J.-M. Guimard[2]

[1] LMT-Cachan, ENS Cachan/CNRS/UPMC/PRES UniverSud Paris, France
feld—allix—baranger@lmt.ens-cachan.fr
[2] EADS France, Innovation Works, Mechanical Modelling Team, France
jean-mathieu.guimard@eads.net

Abstract

This work introduces an enriched description of a mesomodel for laminates in compression. The improvements are based on micromechanical studies of the kinking phenomenon. Several sources of kinking-induced nonlinearities, geometric and material, are selected for integration in the mesomodel. For this purpose, a constitutive homogenization strategy based on energies conservation is proposed and a new energetic potential is defined for the composite ply. The method is illustrated with the full identification of the reponse of a T300/GSL-914C UD ply. Simple laws and couplings are defined and allow for an accurate reproduction the microstructure's behavior. Further, the statistical waviness of the fibers is explicitly integrated in the model and can be used as a probabilistic parameter for mesoscale simulations.

Introduction

The aeronautic industry is continuously introducing long-fiber reinforced composites in increasingly critical components such as shock-absorbers. The main motivation for this application is that laminates, when loaded in compression along the fibers' direction, may break into multiple fragments, in which case they dissipate a large amount of energy [1]. One of the reasons that can explain this high specific absorbed energy is the competition of two highly dissipative degradation mechanisms: delamination between the plies of the composite; and fragmentation of the plies in compression along the fibers' direction. The latter failure mode is mostly due to the microbuckling of the fibers, once the matrix that support them fails, sheared between adjacent fibers [2]. This competition between geometrical and material instability causes the strains to ultimately localize into a characteristic volume of finite width, known as a kink-band. The kinking phenomenon is now widely recognized and understood, thanks to extensive experimental studies (see [3] for a review on fiber waviness for instance).

However, the numerical simulation of kinking is still a challenge due to the difference of scales between that of the phenomena (fiber scale) and that of experimental or numerical testing (sample scale). Computational homogenization strategies, such as the FE^2 method [4, 5], can help bridging

the scales even when nonlinearities occur. Alternatively, using the approach detailed in [6], homogenization can be used to build constitutive laws. An energy equivalence is written between the microstructure and an homogenized model, whose potentials and internal variables must be defined *a priori*. Therefore, the main limitation of this strategy is that the nonlinear mechanisms and their representation at the mesoscale must be identified (see [7]). In this study, we propose to enrich a mesoscale model [8] with results obtained from a previously established microscopic theory [9]. As such, and since we have a rather accurate description of the microscopic phenomena, the method proposed by [6] is chosen for its simplicity and its focus on energy equivalence.

The first part of the paper briefly describes the micromodel used as a reference in this study. Its main characteristics, hypotheses, and results are reminded. Next, the "target" mesomodel and its main existing properties are presented as well. The third chapter is dedicated to a short litterature survey on homogenization techniques for composite materials modeling. Then the numerical strategy considered in this study is presented and applied to a T300/GSL-914C composite. Finally, the possibilities and limits of the method are presented in the light of first results.

1 Microscale theory

The micromodel herein used for the simulation of kinking has been proposed in [9]. Its main hypotheses and results and reminded here. It is a uniaxial microbuckling model based on the *kinking theory* [10], extended to multi-axial loads and with an enriched constitutive behavior for the matrix introducing the effects of fiber/matrix debonding and matrix microcracking. Additional hypotheses include: (1) the RVE is periodic along a β-inclined direction toward the transverse direction, β being the final angle of the kink-band; (2) the fibers are elastic, present a known initial waviness $\overline{\omega}$ (characterized by its amplitude on half-wavelength ratio λ_0), and an Euler-Bernoulli beam-like behavior; (3) the thin matrix is driven by the kinematic of the fibers; (4) buckling is linearized along the mode favored by the waviness shape; (5) the fibers break when a strain-driven brittle criterion is reached, which always occurs post-buckling. This model has been used to simulate the response of a Representative Volume Element Ω made of homogenized fiber-matrix material, loaded in compression $\sigma_{11} \equiv E_1 \varepsilon_{11}$ and/or shear σ_{12} (see Figure 1).

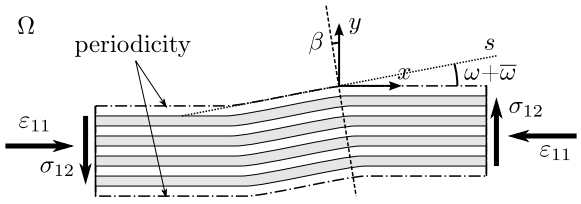

Figure 1: Draft of a RVE representing the material microstructure and loads

A major feature of the model is the introduction of an damageable inelastic behavior for the matrix in shear and transverse tension. It is a critical ingredient for the prediction of compressive strength and absorbed energies. In addition, the response depends strongly on the statistical fiber waviness in terms of critical stresses. Using the largest relastic values of waviness observed by [11], a good correlation between experimental [12, 13] and numerical tests is obtained for critical stresses in a compression-shear plane. On the other hand, the influence of fiber waviness on kink-band size

and absorbed energies has been found of second order, the same as the order of magnitude of scale effects.

2 Mesomodel fundamentals

In order to perform sample-scale comparisons, we wish to include the responses of this micromodel into a higher scale model: the damage mesomodel for laminates developed at the LMT-Cachan (further referenced as *mesomodel* [14, 8]). It is based on two fundamental hypotheses: (1) a laminate's behavior can be derived from that of its plies and interfaces; (2) the degradation state of each ply is constant through-the-thickness and is described using continuum damage mechanics. Let us note 1 the ideal direction of the fibers, 2 the transverse in-plane direction, and 3 the out-of-plane direction. Let us also note σ_{ij} the components of the Cauchy stress tensor and E_i^0, G_{ij}^0, and ν_{ij}^0 the undamaged elastic *moduli* and coefficients of the ply. Finally, d and d' are the damage variables responsible for the influence of diffuse fiber-matrix debonding and matrix micro-cracking on shear and transverse tension, respectively; while d_f is the binary damage representing brittle fiber fracture. The Helmholtz free energy reads:

$$\rho\Psi = \overbrace{\frac{1}{2(1-d_f)}\left(\frac{\langle\sigma_{11}\rangle^2}{E_1^0} + e_c(\langle-\sigma_{11}\rangle)\right)}^{\overline{\Psi}^e} - \sum_{i\neq j}^{\leq 3}\left[\left(\frac{\nu_{ij}^0}{E_i^0} + \frac{\nu_{ji}^0}{E_j^0}\right)\times\sigma_{ii}\sigma_{jj}\right]\Bigg) + \frac{1}{2}\left(\frac{\langle-\sigma_{22}\rangle^2}{E_2^0} + \frac{\langle-\sigma_{33}\rangle^2}{E_3^0}\right)$$
$$+ \frac{1}{2(1-d')}\left(\frac{\langle\sigma_{22}\rangle^2}{E_2^0} + \frac{\langle\sigma_{33}\rangle^2}{E_3^0}\right) + \frac{1}{2(1-d)}\left(\frac{\sigma_{12}^2}{G_{12}^0} + \frac{\sigma_{23}^2}{G_{23}^0} + \frac{\sigma_{31}^2}{G_{31}^0}\right) + \rho\Psi_p(\tilde{p}) \qquad (1)$$

with $\langle.\rangle$ the *positive part* function and $\tilde{p}$ an internal variable describing isotropic inelasticity. The influence of the nonlinear function e_c on compressive failure stress and strain has been experimentally identified in [12] for several composite materials. Here, this function is to be replaced with a micromechanically defined one.

3 Homogenization of composite materials

Homogenization techniques have been used for many years as a modeling tool for increasingly complex microstructures. Most of them are based on the principle of respecting one, several, or preferably all of the following energies: the directly recoverable elastic energy, the energy stored inside the material (as residual self-equilibrated stress and compatible strain fields), and the energy dissipated in heat. To represent the variations of these energies, when they exist, internal variables can be introduced.

Early studies regarding energy storage are due to Taylor and Quinney [15], who investigated the cold work of metals. The extension to cracked materials involving contact with friction is more recent [7]. In [6], the authors detailed a simple theoretical procedure for recovering the stored energy in a more general case, but only applied it in one dimension. More recently, several authors have extended the basic theories and methods previously proposed to the case of brittle or quasi-brittle materials in two dimensions [16]. In [17], such a strategy has been applied to a numerical test case – as opposed to strictly experimental measurements – in order to validate the approach. Similar

procedures have also been applied to carbon-epoxy micro-cracked elementary cells [18], but rather from a damage perspective.

All these approaches are based on similar energy conservation principles. These can be adapted to this case, except that here, the microstructure is considered damageable elastic-plastic and features geometric nonlinearity. As will be shown in the following chapter, similar equivalences and considerations can nevertheless be written. The consistency of the method can be discussed when strong transformation gradients are involved (e.g. close to the edges).

4 Homogenization procedure

The aim of this study is to extract from the micromodel relevant homogenized data in order to feed a mesomodel. The RVE to be homogenized is the volume of material inside the final kink-band. Only two loading directions are considered: compression and shear, possibly mixed. The driving forces are the meso compressive stress σ_{11} and the meso shear stress σ_{12}. In order to identify all the other necessary variables at the mesoscale (internal or observable), energy equivalences similar to those postulated in [7] are considered: The recoverable part of the specific free energy Ψ^e, the stored part of the specific free energy Ψ^p, and the dissipated power Φ are all respected:

$$\Psi^e = \left\langle \Psi^e_\mu \right\rangle_{RVE} \qquad \text{and} \qquad \Psi^p = \left\langle \Psi^p_\mu \right\rangle_{RVE} \qquad \text{and} \qquad \Phi = \left\langle \Phi_\mu \right\rangle_{RVE} \tag{2}$$

where $._\mu$ indicates a microscopic variable and $\langle . \rangle_{RVE}$ is the computed average over the RVE. No initial stresses are considered.

Then, new internal variables have to be introduced. Using the micromodel, the RVE is loaded in pure compression following a cycled path. The result is plotted in Figure 2.a and can be split in two parts: a linear elastic component with a slope equal to the composite's Young modulus (2.b); and a component where all nonlinearities are focused (2.c). On the latter, several sources of nonlinearities are identified: (1) a loss of stiffness, which can be linked to a damage variable d_k; (2) residual strains, which can be linked to inelastic strains ε^p_r; (3) and geometric nonlinear unloadings. Each of them requires a dedicated modelling. Further, geometric nonlinearities will be identified using one strategy and newly introduced internal variables using another.

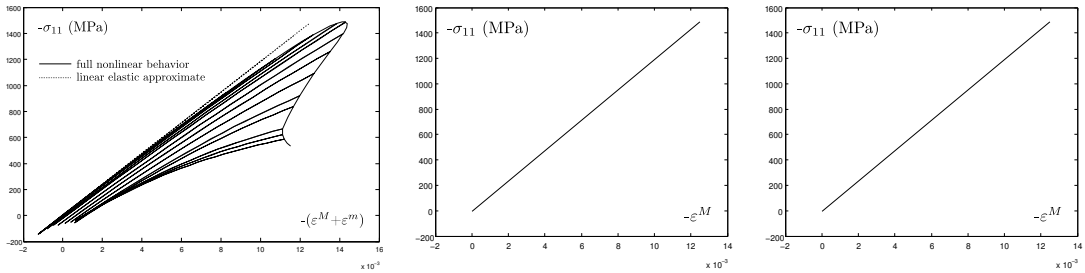

Figure 2: $-\sigma_{11}$ function of $-\varepsilon_{11}$ at the edges of a *kink-band* with a width of 105 μm, a waviness $\lambda_0 = 0.01$, and a shear load $\sigma_{12} = 0$ MPa (left); linear elastic component (center); nonlinear component (right)

If we consider that irreversible strains are driven by a single inelastic variable $\tilde{p}$ (see Section 5.3) and that the strain partition hypothesis holds, the free energy reads $\Psi = \Psi^e(\underline{\underline{\sigma}}, \mathbf{D}) + \Psi^p(\tilde{p})$

where $\mathbf{D}$ is a fourth order damage tensor including d_k. Since the potential depends on several observable and internal variables that evolve with the loading parameter ($\underline{\underline{\sigma}}$), partial derivatives cannot always be computed. Therefore we rely on unloading paths, just like actual experimental tests, where $\frac{d\Psi}{d\underline{\underline{\sigma}}} = \frac{\partial\Psi}{\partial\underline{\underline{\sigma}}}$ and with a direct measure of $\Psi^p(\tilde{p})$ when $\Psi^e = 0$. An identification procedure in two steps featuring several unloadings is set up. First, the elastic nonlinearity is identified on small mixed loads using a minimization technique between the response of the micromodel and a simplified form (described below) for which the nonlinearities also have a geometric origin (Section 5.1). This step has to be repeated for each different microstructure (i.e. waviness value). Then, the damage and inelastic variables' evolution and/or couplings are identified thanks to mixed load paths featuring several unloadings, on which slopes the energies can be recovered (Sections 5.2 and 5.3). This step has *not* to be repeated for different microstructures, as will be shown later, since fiber waviness has been taken into account in the previous step.

The identification of elastic nonlinearities requires an idea of the form the approximation should take. Here a simplified form of the fibrous microstructure is postulated, similar to the early kink-band models for anisotropic rocks [19]. This geometry (see Figure 3) introduces a similar nonlinearity that can nevertheless be directly computed. Note that the "spring" E_1 corresponds to the linear elastic part of the response (Figure 2.b).

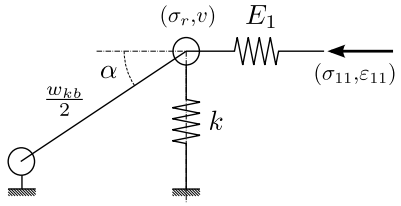

Figure 3: Rheologic draft illustrating the nonlinearity between σ_{11} and ε_{11}

This approximation takes the elastic nonlinearity into account rather simply, assuming α has a non-zero initial value α_0. The mesoscopic compressive stress σ_{11} can then be linked to the mesoscopic compressive strain ε_{11} and each local variable (σ_r, ε_r, ...):

$$v = w_{kb}\left(\frac{1}{2} + \frac{\sigma_{11}}{E_1} - \varepsilon_{11}\right)\tan\alpha = w_{kb}\varepsilon_r + v_0 \qquad \text{and} \qquad \sigma_r = k\varepsilon_r = -\sigma_{11}\tan\alpha \tag{3}$$

5 Identification of a T300/GSL-914C UD ply

5.1 Identification of elastic nonlinearities

Based on the evolution of the elastic strain energy for extremely small mixed loads and various fiber waviness, the values of k and α_0 can be identified. Considering the initial, undamaged value of the spring is a fixed parameter, k^0 is found approximately equal to 18 GPa. The initial defect α_0 is correlated linearly to the fiber waviness λ_0 (see Figure 4.a) and the shear strains (see Figure 4.b) : $\alpha_0 = c_\alpha\lambda_0 + c_\gamma\gamma_{12}$ where $c_\alpha = 12.4$ rd and $c_\gamma = 1.07$ rd.

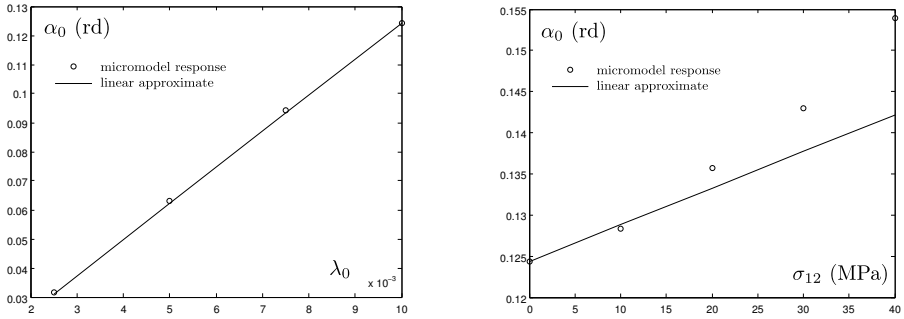

Figure 4: α_0 function of λ_0 (left) and σ_{12} (right)

5.2 Identification of the damage component

The damage variable d_k is defined as the loss of stiffness in the spring k such that $k = k^0(1 - d_k)$. In such conditions, given Equations 1 and 3, the elastic part of the free energy due to kinking reads:

$$\rho\overline{\Psi}^e = \frac{\sigma_{11}^2}{2E_1^0(1-d_f)} + \frac{\sigma_r^2}{2k^0(1-d_k)} \tag{4}$$

The thermodynamic forces associated with shear and kinking damage read:

$$Y_d = -\rho\frac{\partial\Psi}{\partial d} = \frac{1}{2(1-d)^2}\left(\frac{\sigma_{12}^2}{G_{12}^0} + \frac{\sigma_{23}^2}{G_{23}^0} + \frac{\sigma_{31}^2}{G_{31}^0}\right) \qquad \text{and} \qquad Y_r = -\rho\frac{\partial\Psi}{\partial d_k} = \frac{1}{2(1-d_k)^2}\frac{\sigma_r^2}{k^0} \tag{5}$$

However, the results of the micromodel suggest a strong coupling between kinking and shear. Hence, different driving forces are defined in order to couple the associated thermodynamic forces:

$$Y = f_1\left(Y_d + bY_{d'}, Y_r\right) \qquad \text{and} \qquad Y_k = f_2\left(Y_r, Y_d\right) \tag{6}$$

where $b = 0.5$ (already known) is a material parameter, $Y_{d'}$ the thermodynamic force associated with transverse damage, and f_1 and f_2 two functions to be identified. The damage evolution laws are:

$$d = \max_{\tau<t}\left(\frac{\sqrt{Y}-\sqrt{Y_0}}{\sqrt{Y_c}-\sqrt{Y_0}}\right) \qquad \text{and} \qquad d' = cd \qquad \text{and} \qquad d_k = \max_{\tau<t}\left(f_k(Y_k)\right) \tag{7}$$

where $Y_0 = 0.03$ MPa, $Y_c = 8$ MPa, and $c = 0.8$ (already known) are other material parameters and f_k another function to be identified.

The test is first performed without shear loads and considering $Y_k = Y_r$. By loading/unloading increasingly the microstructure, the partial derivative of the elastic free energy is computed for each slope and the damage value can be deduced knowing the undamaged moduli. The results of such a procedure are plotted in Figure 5.a, in terms of damage variable against thermodynamic force. The identification has been repeated for various values of λ_0 and, as expected, the results are rather insensitive.

Once a form for f_k – as simple of complicated as one wishes – is chosen, only f_1 and f_2 remain to be identified. Figures 5.b and 5.c allow for the choice of the following expressions:

$$Y = \left(\sqrt{Y_d + bY_{d'}} + \sqrt{b_r Y_r}\right)^2 \qquad \text{and} \qquad Y_k = Y_r + \sqrt{b_k Y_d} \tag{8}$$

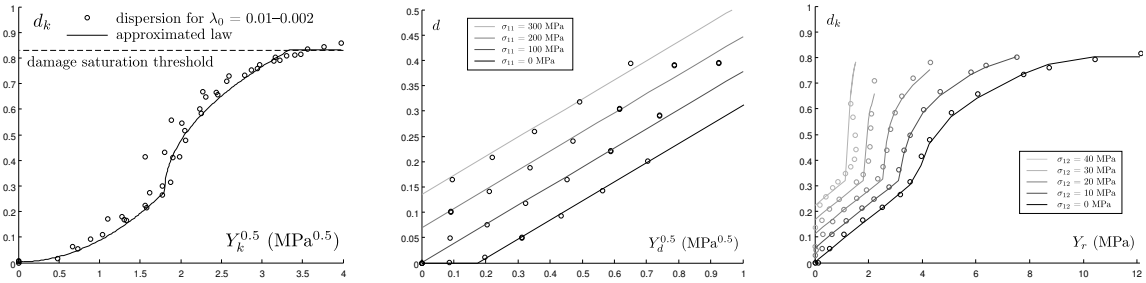

Figure 5: d_k function of $\sqrt{Y_k}$ for $\lambda_0 = 0.01$, 0.0075, 0.005, and 0.0025 (left); d function of $\sqrt{Y_d}$ for varying σ_{11} (center); d_k function of Y_r for varying σ_{12} (right)

where $b_r = 0.12$ and $b_k = 36$ MPa are material parameters. One can also verify that, without compressive stresses, the law linking Y_d to d is the one implemented in the micromodel, which has been chosen compatible with the *mesomodel* in pure shear. The validity of these expressions for large multi-axial loadings is subject to caution.

5.3 Identification of the inelastic component

The development of fiber/matrix debonding and microcracking leads to local slipping between the phases of the composite. At a higher scale, the residual stresses and strains due to these transformations can be seen as material inelasticity. This behavior is best reproduced using "effective" stresses and strains to respect dissipated energy equivalence:

$$\underline{\underline{\tilde{\sigma}}} = (\mathbf{K}^0 : \mathbf{K}^{-1}) : \underline{\underline{\sigma}} \qquad \text{and} \qquad \underline{\underline{\sigma}} : \underline{\underline{\dot{\varepsilon}}}^p = \underline{\underline{\tilde{\sigma}}} : \underline{\underline{\dot{\tilde{\varepsilon}}}}^p \tag{9}$$

The inelastic strain ε_r^p is defined as the irreversible strains in k, such that $\sigma_r = k(\varepsilon_r - \varepsilon_r^p)$. As a first approximation, this strain is considered driven by the same inelastic process as the rest of the mesomodel, under the hypotheses of associated plastic flow and isotropic hardening. The loading surface reads:

$$g(\tilde{\sigma}_{eq}, \tilde{p}) = \tilde{\sigma}_{eq} - \tilde{R}(\tilde{p}) - \tilde{R}_0 \tag{10}$$

with $\tilde{R}_0 = 64$ MPa the initial elastic threshold and $\tilde{R}(\tilde{p}) = \rho \frac{\partial \Psi}{\partial \tilde{p}} = K_p \tilde{p}^{m_p}$ where $K_p = 1000$ MPa and $m_p = 0.54$ are previously identified parameters (on $\pm 45°$ tensile tests). Finally, $\tilde{\sigma}_{eq}$ is an equivalent stress and is the single parameter of the model that can actually be modified if all other hypotheses are to be respected. After each computation of the elastic and damageable components, under the strain partition hypothesis, the stored and dissipated energies of the model can be computed using Equations 2. The results are plotted in Figure 6.a. The evolution presents an unusual shape that can be approximated with:

$$\tilde{\sigma}_{eq} = \sqrt{\tilde{\sigma}_{12}^2 + a^2 \tilde{\sigma}_{22}^2} + a_r \tilde{\sigma}_r \tag{11}$$

where $a = 0.5$ (already known) and $a_r = 0.25$ are coupling coefficients.

These choices allow for a good representation of the evolution law up to a certain point. Hence, we define a saturation criterion for inelasticity: $\dot{\tilde{p}} = 0$ when $a_r \tilde{\sigma}_r > \sigma_T$, with $\sigma_T = 95$ MPa. Again, as expected, the variability introduced by fiber waviness does not significantly affect the shape.

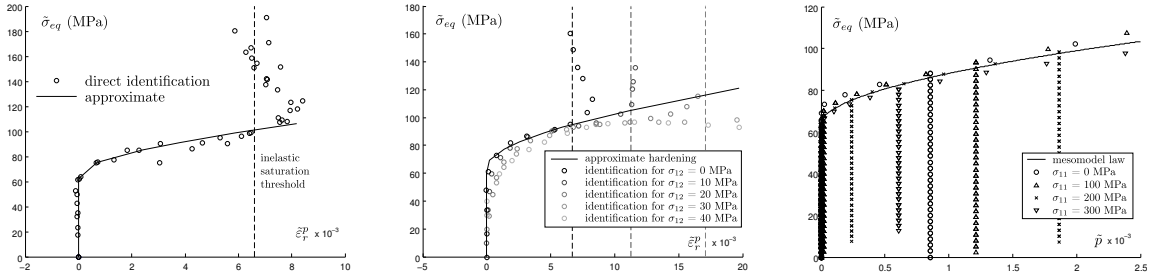

Figure 6: $\tilde{\sigma}_{eq}$ function of $\tilde{\varepsilon}^p_r$ for $\lambda_0 = 0.01$, 0.0075, 0.005, and 0.0025 (left) and for various σ_{12} (center); $\tilde{\sigma}_{eq}$ function of $\tilde{p}$ for varying σ_{11} (right)

Figure 6.b also reveals a good reproduction of compression loadings preceded by shear, with the saturation threshold moving as the compressive criterion is reached "later" on the graph. Similarly, Figure 6.c displays a good reproduction of shear loadings preceded by compression, without any saturation threshold. Consequently, the hypothesis of "kinking-driven" inelasticity following the same process as the rest of the mesomodel is verified. The only unexpected ingredient is the cumulated inelasticity threshold, but since its criterion is strictly compression-driven, it does not change standard results in other directions. Once again, the validity of these expressions for large multi-axial loadings is subject to caution.

6 Conclusion

With all necessary parameters of the model identified, this method offers a good reproduction of the microstructure compressive behavior up to complete failure, as Figure 7.a shows. Nonlinear mechanisms are reproduced and the error in terms of stored and dissipated energies is of the order of magnitude of the percent. The results are less accurate but acceptable when the waviness evolves and under mixed loadings, as Figures 7.b and 7.c show.

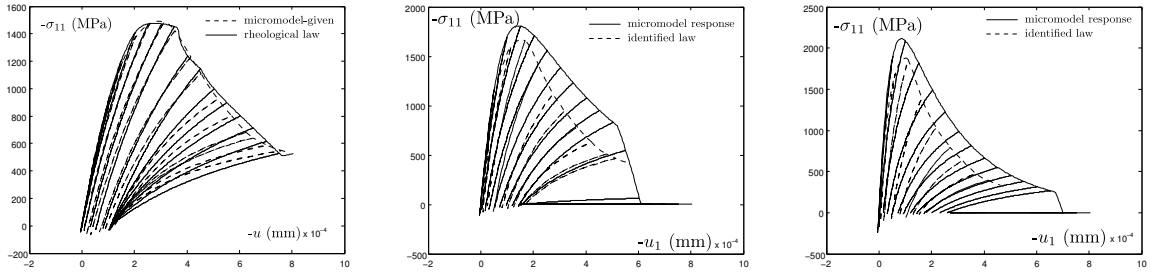

Figure 7: Stress-strain constitutive law identified at the edges of the *kink-band* for $\lambda_0 = 0.01$ and $\sigma_{12} = 0$ MPa (left); $\lambda_0 = 0.0075$ and $\sigma_{12} = 20$ MPa (center); $\lambda_0 = 0.005$ and $\sigma_{12} = 30$ MPa (right)

The implementation of the identified laws in any version of the *mesomodel* will allow for three dimensional simulations up to failure to be performed. However, a few precautions have to be

taken for the numerical integration of the full constitutive law when the bulk elastic component is added. Because of the snap back, the solution of the constitutive law is not always unique. In an implicit case, a combination of continuation algorithms may be used to follow the solution and the equilibrium paths at all time. In an explicit framework, the least precaution to take is to accurately compute the released, stored, and dissipated energies during stress jumps.

Acknowledgement

This work has been carried out in the framework of the ANR *VulComp* Phase 1 project, under the grant ANR-2006-MAPR-0022-01, whose financial support is gratefully acknowledged.

References

[1] Alastair F. Johnson and Anthony K. Pickett. Impact and crash modelling of composite structures: A challenge for damage mechanics. In *ECCM 99*, Munich, 1999.

[2] Ali S. Argon. Fracture of composites. *Treatise on Materials Science and Technology*, 1:79–114, 1972.

[3] Michael R. Piggott. The effect of fibre waviness on the mechanical properties of unidirectional fibre composites: a review. *Composites science and technology*, 53(2):201–205, 1995.

[4] Frédéric Feyel and Jean-Louis Chaboche. Fe2 multiscale approach for modelling the elastoviscoplastic behaviour of long fibre sic/ti composite materials. *Computational Methods in Applied Mechanics and Engineering*, 183:309–330, 2000.

[5] S. Nezamabadi, J. Yvonnet, H. Zahrouni, and M. Potier-Ferry. A multilevel computational strategy for handling microscopic and macroscopic instabilities. *Computational Methods in Applied Mechanics and Engineering*, 198:2099–2110, 2009.

[6] N. Aravas, K.-S. Kim, and F. A. Leckie. On the calculations of the stored energy of cold work. *Journal of Engineernig Materials and Technology*, 112:465–470, 1990.

[7] Stéphane Andrieux, Yves Bamberger, and Jean-Jacques Marigo. Un modèle de matériau microfissuré pour les bétons et les roches. *Journal de Mécanique Théorique et Appliquée*, 5(3):471–513, 1986.

[8] Pierre Ladevèze and Éric Le Dantec. Damage modeling of the elementary ply for laminated composites. *Composites Science and Technology*, 43(3):257–267, 1992.

[9] Nicolas Feld, Olivier Allix, Emmanuel Baranger, and Jean-Mathieu Guimard. Micro-mechanical prediction of ud laminates behaviour under combined compression up to failure: influence of matrix degradation. *Journal of Composite Materials*, doi: 10.1177/0021998311401084, 2011.

[10] Bernard Budiansky and Norman A. Fleck. Compressive failure of fiber composites. *Journal of the Mechanics and Physics of Solids*, 41(1):183–211, 1993.

[11] Bernard Paluch. Analysis of geometric imperfections in fibres for unidirectional fibre-reinforced composites. *La Recherche Aéronautique*, 6:431–448, 1994.

[12] Olivier Allix, Pierre Ladevèze, and Éric Vittecoq. Modelling and identification of the mechanical behaviour of composite laminates in compression. *Composites Science and Technology*, 51(1):35–42, 1994.

[13] Mike J. Hinton, A. Sam Kaddour, and Peter D. Soden, editors. *Failure Criteria in Fibre Reinforced Polymer Composites: The World-Wide Failure Exercise*. Elsevier Science, 2004.

[14] Olivier Allix and Pierre Ladevèze. Interlaminar interface modelling for the prediction of delamination. *Composite Structures*, 22(4):235–242, 1992.

[15] G. I. Taylor and H. Quinney. The latent energy remaining in a metal after cold working. *Proceedings of the Royal Society of London - Series A*, 143(849):307–326, 1934.

[16] François Hild, Alain Burr, and Frederick A. Leckie. Matrix cracking and debonding of ceramic-matrix composites. *International Journal of Solids and Structures*, 33(8):1209–1220, 1996.

[17] G. Vivier, H. Trumel, and François Hild. On the stored and dissipated energies in heterogeneous rate-independent systems: theory and simple examples. *Continuum Mechanics and Thermodynamics*, 20(7):411–427, 2009.

[18] Pierre Ladevèze and Gilles Lubineau. An enhanced mesomodel for laminates based on micromechanics. *Composites Science and Technology*, 62(4):533–541, 2002.

[19] A. J. Baer and D. K. Norris, editors. *Research in Tectonics: Kink Bands and Brittle Deformation*, Ottawa, March 1968. Geological Survey of Canada. GSC Paper 68-52.